Performance Analysis of a Closely Coupled GPS/INS Relative Positioning Architecture for Automated Ground Vehicle Convoys

William Travis and David M. Bevly
GPS and Vehicle Dynamics Lab, Auburn University

BIOGRAPHY

William Travis is a graduate student at Auburn University in Auburn, Alabama studying ground vehicle navigation. He graduated with a B.S. in Mechanical Engineering in 2004 and a M.S. in Mechanical Engineering in 2006, both from Auburn University. He was a member of and developed the navigation system for the 2005 SciAutonics-Auburn Engineering DARPA Grand Challenge team. Currently, he is investigating relative positioning strategies for ground vehicle convoys.

Dr. David M. Bevly received his B.S. from Texas A&M University in 1995, M.S from Massachusetts Institute of Technology in 1997, and Ph.D. from Stanford University in 2001 in mechanical engineering. He joined the faculty of the Department of Mechanical Engineering at Auburn University in 2001 as an assistant professor. Dr. Bevlys research interests include control systems, sensor fusion, GPS, state estimation, and parameter identification. His research focuses on vehicle dynamics as well as modeling and control of vehicle systems. Additionally, Dr. Bevly has developed algorithms for navigation and control of off-road vehicles and methods for identifying critical vehicle parameters using GPS and inertial sensors.

ABSTRACT

A relative positioning software architecture incorporating inertial, range, and phase measurements has been developed to enhance the ability and accuracy of path following for autonomous ground vehicles in a convoy. GPS carrier measurements are fused with INS systems on board each vehicle to exploit the temporal and spacial error correlation of GPS signals within the same region and determine a high precision relative position vector between moving vehicles in the convoy. A discussion of the difficulties encountered in a ground vehicle environment is presented, along with the derivation of the algorithms to run on the convoy vehicles. An increase in robustness to the position solution is seen, and the relative position solution shows the ability to bridge short GPS outages.

INTRODUCTION

The ability to precisely follow another vehicle with large separation distances would have an immediate impact on ground vehicle systems operated by the military and future automated civilian vehicle systems. A convoy of unmanned ground vehicles (UGVs) could be controlled by a single driver and operational efficiency could be improved by freeing more personnel to handle other tasks. In high risk scenarios, such as traveling through a field with unexploded ordinance (UXO), safety could be improved by having a fleet of vehicles replicate the path driven by a mine clearing vehicle or a vehicle with an on-board UXO detection system.

Previous work has shown the feasibility of using an accurate relative position vector to provide a means for following vehicles to accurately duplicate a lead vehicle's path of travel instead of maintaining a fixed formation [1]. This ability could play a crucial role in both civilian, agricultural, and military systems by allowing one driver to operate a fleet of vehicles. Current applications using relative positioning technology can be seen in the areas of formation flight [2, 3]; automated aircraft refueling (AAR) [4, 5]; the Joint Precision Approach and Landing System (JPALS) [6, 7]; and ship flexure measurement [8].

Due to the operating environment of ground vehicles, GPS outages, multipath, and cycle slips have a higher frequency of occurrence than aerial vehicle applications. Incorporating inertial systems into the relative positioning algorithms can mitigate these effects and improve the robustness of the relative positioning solution [9]. Also, the addition of the inertial systems can reduce the data transmission requirements for the relative navigation system by increasing the required time between GPS observation updates while still maintaining a high rate solution.

The paper is outlined as follows:

- A description of the GPS observation models to establish concepts and equations referenced throughout the paper.
- Relative positioning utilizes measurements from multiple receivers. A brief overview of the formation of relative range and phase measurements is given.
- The challenges of operating in a ground vehicle environment are discussed. These challenges are not necessarily unique, but the frequency and sudden severity can hinder navigation systems.
- Various GPS/INS integration methods are presented in order to justify the reasoning for choosing a closely coupled integration scheme. The algorithms used to determine a stand alone and relative position solution are provided.
- Results of the algorithm are presented, which include several plots displaying the robustness improvement and high rate solution. GPS outages are simulated to assess the relative positioning algorithm when forced to dead reckon. For seven outages, the mean time taken to drift beyond 10cm was 3.97 seconds using two automotive grade IMUs.

OBSERVATION MODELS

Ranging information is output from a GPS receiver in the form of pseudo-range, carrier phase, and Doppler frequency measurements. The broadcast GPS signal is corrupted by atmospheric effects, obstructions, and reflection before it reaches the receiver. Satellite and receiver clock biases add uncertainty to the transmission and arrival times assigned to samples of the signal. These errors degrade the accuracy of the receiver generated range information, hence the term "pseudo-range". Fortunately, the error sources can be independently added to the true value to produce a simple but effective measurement model. Expressions for the measured pseudo-range, carrier phase, and Doppler frequency are shown below [10], with variable definitions given in Table 1.

$$\begin{aligned}\rho_A^j(t_k) =& \|\vec{r}_A^j(t_k)\| + \gamma(t_k) + \xi(t_k) + c\delta t_A(t_k) \\ & - c\delta t^j(t_k) + \epsilon_\rho(t_k)\end{aligned} \tag{1}$$

$$\begin{aligned}\phi_A^j(t_k) =& \|\vec{r}_A^j(t_k)\| - \gamma(t_k) + \xi(t_k) + \lambda N_A^j(t_k) \\ & + c\delta t_A(t_k) - c\delta t^j(t_k) + \epsilon_\phi(t_k)\end{aligned} \tag{2}$$

$$f_{D_A}^j = -\frac{\|\dot{\vec{r}}_A^j(t_k)\|}{\lambda} + \epsilon_f(t_k) \tag{3}$$

The availability of two range measurements seems redundant until their individual contributions are assessed. The pseudo-range measurement is a direct measurement of

Table 1 Observation Model Variables

Variable	Description	Units
ρ_A^j	the measured range (pseudo-range) from receiver A to satellite j	m
ϕ_A^j	the measured carrier signal phase from receiver A to satellite j	m
$f_{D_A}^j$	the measured Doppler shift from receiver A to satellite j	cycles
$\vec{r}_A^j$	the true range vector from satellite j to receiver A	m
$\dot{\vec{r}}_A^j$	the true range rate vector from satellite j to receiver A	m/s
λ	the wavelength of the carrier	m
γ	the ionospheric delay/advancement	m
ξ	the tropospheric delay	m
δt_A	the clock error at the receiver	s
δt^j	the clock error at satellite j	s
N_A^j	the integer number of cycles from receiver A to satellite j	cycles
ϵ	system noise, including multipath	m

user to satellite range, while the carrier measurement contains an unknown range bias known as the integer ambiguity. A receiver tracks the phase of the received signal when a GPS satellite comes into view, but the integer number of cycles of the carrier at the commencement of tracking remains unknown. The carrier phase measurement is of a higher quality than the pseudo-range measurement. Typical accuracies for pseudo-range measurements are half a meter, while accuracies for the phase measurement are around five millimeters [10]. The phase measurement is also more robust to multipath error [11].

The Doppler measurement is a function of the receiver to satellite range rate. Terms indicating the time rate of change of the atmospheric errors were not included in Equation 3 because the errors were assumed to be nearly constant from one epoch to the next. Manipulation of the equation produces a pseudo-range rate expression.

$$\dot{\rho}_A^j = -\lambda f_{D_A}^j \tag{4}$$

Measurement accuracy is determined by the bandwidth of receiver's tracking loops, signal quality, and anticipated multipath effects. Expressions of the accuracy of the phase, delay, and frequency lock loops (PLL, DLL, and FLL, respectively) as a function of the carrier to noise ratio, C/N_0, expressed in Hertz, are given in [10] and [12].

$$\sigma_{tDLL} = \lambda_c\sqrt{\frac{4d^2 B_{n\rho}}{C/N_0}\left(2(1-d) + \frac{4d}{T_s C/N_0}\right)} \tag{5}$$

$$\sigma_{tPLL} = \frac{\lambda}{2\pi}\sqrt{\frac{B_{n\phi}}{C/N_0}\left(1 + \frac{1}{T_s C/N_0}\right)} \tag{6}$$

$$\sigma_{tFLL} = \frac{\lambda}{2\pi T_s}\sqrt{\frac{4B_{n\rho}}{C/N_0}\left(1 + \frac{1}{T_s C/N_0}\right)} \tag{7}$$

The measurement errors consist of the tracking loop errors plus additional terms. The terms κ_ρ and κ_ϕ are used to inflate the error bounds to account for unmodeled terms, such as multipath and any residual atmospheric effects.

$$\sigma_{\epsilon_\rho} = \kappa_\rho + \sigma_{tDLL} \tag{8}$$

$$\sigma_{\epsilon_\phi} = \kappa_\phi + \sigma_{tPLL} \tag{9}$$

$$\sigma_{\epsilon_{\dot\rho}} = \sigma_{tFLL} + f_e/3 \tag{10}$$

Tracking loop parameters are receiver dependent, but approximations were used in this work based on those given in [12]. Values are listed in Table 2.

Table 2 Tracking Loop Parameters

Parameter	Value	Unit
$B_{n\rho}$, code loop noise bandwidth	2	Hz
$B_{n\phi}$, carrier loop noise bandwidth	18	Hz
d, correlator spacing	0.5	chips
f_e, dynamic stress error	3	m/s
κ_ρ, unmodeled range error,	5	m
κ_ϕ, unmodeled phase error,	0.02	m
λ, carrier wavelength	0.1902	m
λ_c, code chip width	293.05	m
T_s, predetection integration time	0.005	s

RELATIVE POSITION

The error terms in the range measurements are correlated in time and space. Therefore, two receivers in close proximity are nearly identically affected by many of the error sources. A Real-Time Kinematic (RTK) system is a form of differential GPS (DGPS) that differences out the common mode errors between multiple GPS receivers in close proximity (<20 km) to obtain a high accuracy position solution. A static receiver is set up at a base station with a known location. A relative position vector (RPV), or baseline vector, is determined with high accuracy between the base station and a dynamic receiver by processing GPS range measurements. The RPV is then added to the known position of the base station to produce a highly accurate global position solution. A dynamic base RTK (DRTK) system operates on the same principles; the RPV between two moving receivers is estimated. The accuracy of the RPV is retained, but the global position accuracy is not.

A simple subtraction of the measurements across the two receivers mitigates the ionospheric, tropospheric, and satellite clock terms [13]. This is known as a single difference. Single differenced range and phase measurements are expressed as follows:

$$\Delta\rho^j_{AB}(t_k) = \rho^j_B(t_k) - \rho^j_A(t_k) \tag{11}$$

$$\Delta\phi^j_{AB}(t_k) = \phi^j_B(t_k) - \phi^j_A(t_k) \tag{12}$$

The result of a single difference is a range measurement between receivers associated with one satellite. The lingering error terms are receiver clock biases, an increased noise, and the ambiguity on the phase measurement. Note the new ambiguity is a function of the two original receiver to satellite ambiguities.

One single difference measurement, preferably of high quality and likely to remain in sight, is selected as a base measurement. From it, each of the other single differenced measurements are subtracted to form a double differenced measurement. This action removes the receiver clock bias error.

$$\begin{aligned}\nabla\Delta\rho^{jz}_{AB}(t_k) =& \Delta\rho^z_{AB}(t_k) - \Delta\rho^j_{AB}(t_k)\\ =& \|\vec{r}_{AB}(t_k)\| + \epsilon_{\nabla\Delta\rho}(t_k)\end{aligned} \tag{13}$$

$$\begin{aligned}\nabla\Delta\phi^{jz}_{AB}(t_k) =& \Delta\phi^z_{AB}(t_k) - \Delta\phi^j_{AB}(t_k)\\ =& \|\vec{r}_{AB}(t_k)\| + \lambda N^{jz}_{AB} + \epsilon_{\nabla\Delta\phi}(t_k)\end{aligned} \tag{14}$$

A variety of combinations using these measurements can be made to form wide lane, narrow lane, ionosphere free, etc. observables, which are used to estimate the RPV and ambiguities. A summary of some of the combinations can be found in [14] and [5].

The estimated ambiguities and their respective error covariance is used to fix the estimates to integer values. One widely used fixing routine is the LAMBDA method [15], although many others exist [11]. Once the integer valued ambiguities are determined with a sufficient probability of being correct, they are removed from the phase observable to produce a precise range measurement. The phase based range measurement is re-processed to determine a high accuracy RPV.

IMPLEMENTATION CHALLENGES

The prevelency and persistency of challenges presented by the ground vehicle operational environment create difficulties when determining an accurate and consistent GPS based navigation solution. The challenges are enhanced when attempting to simultaneously process measurements from multiple non-colocated receivers as the local environment around each receiver is unique. Effects such as shadowing and multipath obfuscate the independently received signals and the resulting accuracy of the measurements, reducing the ability to estimate the ambiguities with sufficient accuracy for integer fixing. The low elevation of the antenna increases the likelihood and frequency of objects obscuring the lines of sight between it and satellites. Therefore, partial outages can be common. Also, consistency of observations is not guaranteed. A receiver might track four satellites, but it might not track the same four from epoch to epoch. The probability of two receivers observing the same satellites, which is necessary to obtain a DRTK solution, can be low in such situations.

Frequent outages also reduce the feasibility of some techniques used to enhance the accuracy of the ambiguity estimate. For instance, the JPALS algorithm as described in [5] computes a geometry-free wide-lane observable. This observable is inherently noisy, but it is very stable. It is passed through a moving average filter before insertion into the estimation algorithm to remove the noise. This computation results in a very stable, multipath free ambiguity measurement. However, this is not feasible on a ground vehicle because many operational scenarios that create frequent outages would reduce the effectiveness of the moving average filter.

Figure 1 displays the L1 observations and associated C/N_0 of a single NovAtel PropakV-3 receiver on a passenger vehicle in a typical suburban environment. The vehicle was static for the first 100 seconds, where the receiver consistently tracked nine satellites and the C/N_0 was reasonably high. Once the vehicle started traveling, it traveled under overhanging trees, signs, and up to four story buildings. The vehicle came to rest between two story buildings. The number of observations fluctuated between three and ten satellites as the vehicle traveled. Also, the reported signal quality for many of the satellites was quite poor, with only three observations having a C/N_0 above 40 dB-Hz at the end of the run.

INS INTEGRATION OPTIONS

A natural addition to aid the fluctuations in the GPS range measurements are inertial measurements. GPS and inertial systems are often fused together to produce a high rate, smooth navigation solution capable of dead reckoning through short GPS outages. The same idea can be employed to combat the environmental impact; relative inertial measurements can dead reckon through intermittent outages and smooth jumps in the RPV solution created by frequently changing observations. The GPS and INS data can be fused using several methods, so consideration to multiple methods was given to determine the most efficient integration routine.

Combining the raw inertial data with the GPS relative range data poses a problem because inertial data from each vehicle will be non-coincident. The data must be aligned before it can be differenced to produce relative inertial data. Furthermore, the relative inertial data must be expressed in the navigation frame before it can be integrated to produce relative velocity and position information. Pre-processing the inertial data on each vehicle can calibrate and rotate the inertial data into a navigation frame common among all vehicles.

Three integration strategies are defined in [13]: uncoupled, loosely coupled, and tightly coupled integration. Uncoupled and loose coupling fuse inertial data with position and velocity data computed by the receiver to form a navigation solution. These two techniques are relatively simple to implement. The difference between the two methods is loose coupling provides feedback into the INS to correct errors. Loose integration can also feedback the solution into the receiver to aid its tracking loops. The inherent drawback to these methods is the rejection of information when the GPS receiver is incapable of producing a solution. Often, the receiver is still tracking some satellites, but any information is not utilized.

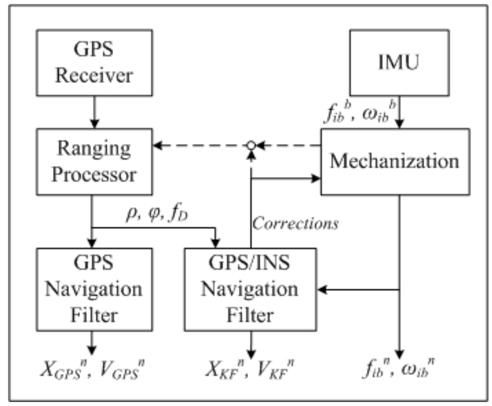

Fig. 2 A closely coupled integration algorithm fuses inertial data with GPS range data to produce a navigation solution. The dashed line represents the option to aid the receiver tracking loops with the inertial and navigation data.

A tightly coupled system processes the inertial data with range measurements to each satellite and aids the receiver tracking loops with the position solution. A derivative of this fusion method was implemented; a closely coupled system does not aid the tracking loops but still processes the inertial and range data to produce a navigation solution. Figure 2 is a block diagram depicting a closely/tightly coupled system. The IMU is mechanized and produces measurements in a navigation frame before combining with inertial data. The dashed line represents feedback to the receiver tracking loops, which was not implemented in this work.

The closely coupled routine was chosen to pre-process the inertial data on each vehicle prior to forming any relative measurements. The measurements are placed in a common navigation frame, which was chosen to be the Earth centered, Earth fixed (ECEF) frame, in the mechanization process. An added benefit is the availability of a high rate, robust position solution to each vehicle and its subsystems.

Once the relative inertial data is obtained, one must decide how to best couple it with the relative range measurements to aid the relative position solution. The same two basic options are presented: loose or close coupling. A loose coupling algorithm would combine the output of the DRTK algorithm with the relative inertial data to provide some filtering and a high rate RPV. However, this approach does not contribute to the integrity of the ambiguity estimates as only the corrupted range measurements are available in the DRTK algorithm. A close coupling approach provides more information about the motion of the two vehicles, so emphasis on potentially degraded relative range measurements can be lowered. This has a direct impact on the ambiguity estimates. Also, the close coupling approach

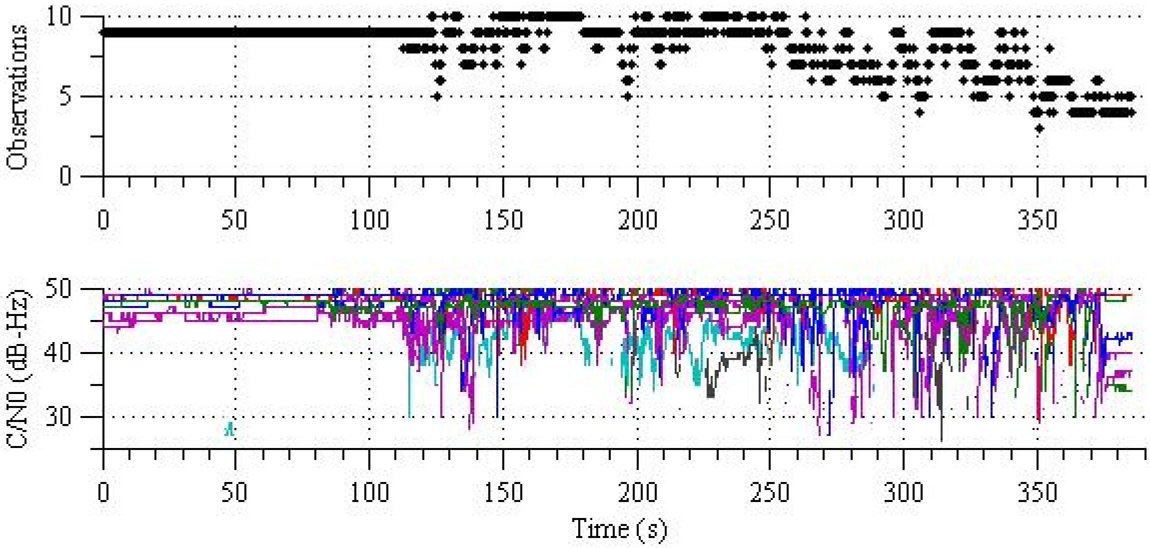

Fig. 1 The observations and associated C/N_0 of a single receiver traveling through a suburban environment are shown. The observations are inconsistent from epoch to epoch and the signal quality degrades from shadowing and multipath, reducing the ability to accurately estimate phase ambiguities.

can offer a graceful solution degradation in the event of a severe or full outage.

GPS/INS INTEGRATION

The inertial measurements were mechanized to determine the specific force vector in the ECEF frame, $\vec{f}^e$. The expression is reliant upon the Euler angles from the inertial frame to the ECEF frame, ϕ, θ, and ψ; the receiver position vector in the ECEF frame, $\vec{p}^e_{eb}$; the receiver velocity vector in the ECEF frame, $\vec{v}^e_{eb}$; accelerometer bias, b_{f_k}; and the Earth's rotational rate expressed in skew-symmetric form, Ω^e_{ie}.

$$\vec{f}^e_k = C^e_b(\vec{f}^b_k - b_{f_k}) + G(\vec{p}^e_{eb_{k-1}}) - 2\Omega^e_{ie}\vec{v}^e_{eb_{k-1}} \tag{15}$$

The rotation matrix from the body to ECEF frame is denoted by C^e_b and defined below ($c[\bullet]$ and $s[\bullet]$ are the cosine and sine of an angle).

$$C^e_b = \begin{bmatrix} c\theta c\psi & -c\phi s\psi + s\phi s\theta c\psi & s\phi s\psi + c\phi s\theta c\psi \\ c\theta s\psi & c\phi c\psi + s\phi s\theta s\psi & -s\phi c\psi + c\phi s\theta s\psi \\ -s\theta & s\phi c\theta & c\phi c\theta \end{bmatrix} \tag{16}$$

The gravity model computed the gravitational and centripetal effects at the user position.

$$G(\vec{p}^e) = -\frac{GM}{\|\vec{p}^e_{eb}\|^3}\vec{p}^e_{eb} - \Omega^e_{ie}\Omega^e_{ie}\vec{p}^e_{eb} \tag{17}$$

The vectors containing the position, velocity, and Euler angles are discretely propagated, where Δt is the IMU sample rate, as follows:

$$\vec{p}^e_{eb_k} = \vec{p}^e_{eb_{k-1}} + \vec{v}_{eb_{k-1}}\Delta t + \vec{f}^e_k\frac{\Delta t^2}{2} \tag{18}$$

$$\vec{v}^e_{eb_k} = \vec{v}^e_{eb_{k-1}} + \vec{f}^e_k\Delta t \tag{19}$$

$$\vec{a}_k = \vec{a}_{k-1} + M^e_b(\omega^b_{ib_k} - b_{g_k})\Delta t \tag{20}$$

where ω^b_{ib} is the rotation rate measured in the body frame, b_{g_k} contains the rate gyroscope biases, and

$$M^e_b = \begin{bmatrix} 1 & \frac{s\phi s\theta}{c\theta} & \frac{c\phi s\theta}{c\theta} \\ 0 & c\phi & -s\phi \\ 0 & \frac{s\phi}{c\theta} & \frac{c\phi}{c\theta} \end{bmatrix} \tag{21}$$

The receiver clock bias is propagated using the estimated clock drift.

$$c\delta t_{u_{k+1}} = c\delta t_{u_k} + c\dot{\delta t}_{u_{k+1}}\Delta t \tag{22}$$

White noise is assumed to drive the bias and clock drift states. With this assumption and the above expressions, the estimated state vector is defined as follows:

$$X = \begin{bmatrix}\vec{p}^e & \vec{v}^e & \vec{a} & b_f & b_g & c\delta t & c\dot{\delta t}\end{bmatrix}^T \tag{23}$$

The estimates are propagated forward in time when IMU data is available using the nonlinear relationships given in Equations 15-22.

$$X^-_k = f\left(X^+_{k-1}, f^b_k, w^b_{ib_k}, \Delta t\right) \tag{24}$$

The state transition matrix, Φ, is determined by calculating the Jacobian of $f\left(X, f^b, w^b_{ib}, \Delta t\right)$ with respect to the state vector, X. Process covariance matrix containing the of sensor noise and bias drift, which is a function of IMU quality, is given by the following expression:

$$Q_1 = diag\left(\begin{bmatrix}\sigma^2_f & \sigma^2_g & \sigma^2_{bf} & \sigma^2_{bg}\end{bmatrix}\right) \tag{25}$$

The covariance of the receiver clock states is derived in [16].

$$Q_2 = \begin{bmatrix} S_b \Delta t + S_f \frac{\Delta t^3}{3} & S_f \frac{\Delta t^2}{2} \\ S_f \frac{\Delta t^2}{2} & S_f \Delta t \end{bmatrix} \tag{26}$$

Together, the process covariance matrix is formed.

$$Q = \begin{bmatrix} Q_1 & 0 \\ 0 & Q_2 \end{bmatrix} \tag{27}$$

The gain matrix relating the process noise to the state vector is determined by calculating the Jacobian of $f\left(X, f^b, w_{ib}^b, \Delta t\right)$ with respect to a vector containing the process noise. The error covariance estimate is propagated in time as follows:

$$P_k^- = \Phi_k P_{k-1}^+ \Phi_k^T + \Upsilon Q \Upsilon^T \tag{28}$$

Measurements in the closely coupled system consist of the range information computed in the GPS receiver. Specifically, the pseudo-range and pseudo-range rate are used. The phase information can be used in lieu of the pseudo-range rate, but using both does not add information to the system because the phase measurement is the integral of the Doppler shift. The measurement vector is denoted by z.

$$z = \begin{bmatrix} \rho & \dot{\rho} \end{bmatrix}^T \tag{29}$$

The relationship between the states and measurements is nonlinear.

$$h(X) = \begin{bmatrix} \sqrt{\left[\vec{p}_{eb}^e - \vec{p}_{es}^e\right]^T \left[\vec{p}_{eb}^e - \vec{p}_{es}^e\right]} + c\delta t \\ \frac{\left[\vec{p}_{eb}^e - \vec{p}_{es}^e\right]^T \left[\vec{v}_{eb}^e - \vec{v}_{es}^e\right]}{\sqrt{\left[\vec{p}_{eb}^e - \vec{p}_{es}^e\right]^T \left[\vec{p}_{eb}^e - \vec{p}_{es}^e\right]}} + c\delta \dot{t} \end{bmatrix} \tag{30}$$

The measurement matrix is formed by calculating the Jacobian of $h(X)$ with respect to the state vector. The elements relating the velocity measurement to the position state were assumed to be zero.

$$H = \begin{bmatrix} e_b^s & 0 & 0 & 0 & 0 & 1 & 0 \\ 0 & e_b^s & 0 & 0 & 0 & 0 & 1 \end{bmatrix} \tag{31}$$

In the above expression, e_b^s denotes the unit vector from the receiver to the satellite. The measurement covariance matrix was determined using the values obtained from Equations 8 and 10. Measurements were assumed to be uncorrelated.

The Kalman gain and measurement updates are computed when measurements are output by the receiver.

$$K = P_k^- H^T \left(H P_k^- H^T + R\right)^{-1} \tag{32}$$

$$X_k^+ = X_k^- + K\left(z - h(X_k^-)\right) \tag{33}$$

$$P_k^+ = (I_{17} - KH) P_k^- \tag{34}$$

GPS data collected during the test depicted in Figure 1 was processed along with data from a Crossbow IMU440.

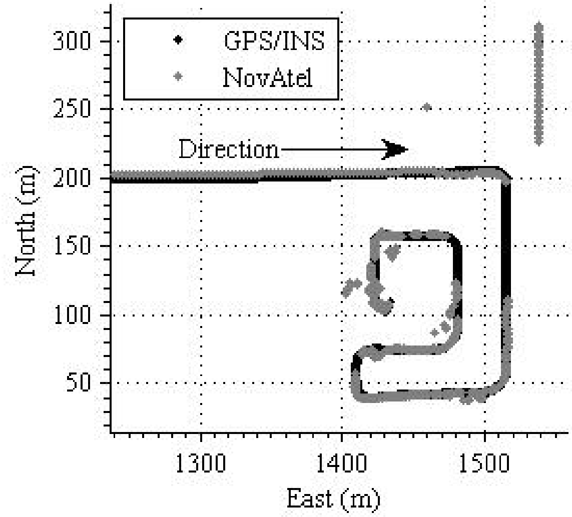

Fig. 3 The closely coupled solution is superior to a stand alone solution in a suburban environment due to its ability to de-weight potentially erroneous measurements more effectively.

The data was combined in the closely coupled algorithm described above. Figure 3 shows position data from the NovAtel and the navigation solution from the closely coupled algorithm which corresponds to Figure 1 from 250 seconds to the end of the run. The output, originally in the ECEF frame, has been placed into a local North, East, Down (NED) frame for clarity. The inertial data clearly improves the solution by mitigating substantial jumps in position as the vehicle traveled between multiple two story buildings.

DRTK/INS INTEGRATION

The closely coupled system on board each vehicle processes pseudo-range and pseudo-range rate data with inertial data to produce a position solution. The specific force in the navigation frame is a by-product of the coupling routine, and it can be combined with specific force measurements from other locations if they are in the same frame. The result is the relative acceleration between multiple points in the navigation frame, or the second derivative of the RPV with respect to time.

$$\Delta f_{AB}^e = f_B^e - f_A^e \tag{35}$$

A block diagram of the DRTK/INS architecture is shown in Figure 4. Again, each vehicle produces its own navigation solution with the GPS and inertial measurements. The lead vehicle then transmits its specific force measurement with any available range measurements to other vehicles, where the RPV is then computed.

Feedback was added to the relative INS system to compensate for any residual biases. The RPV equation con-

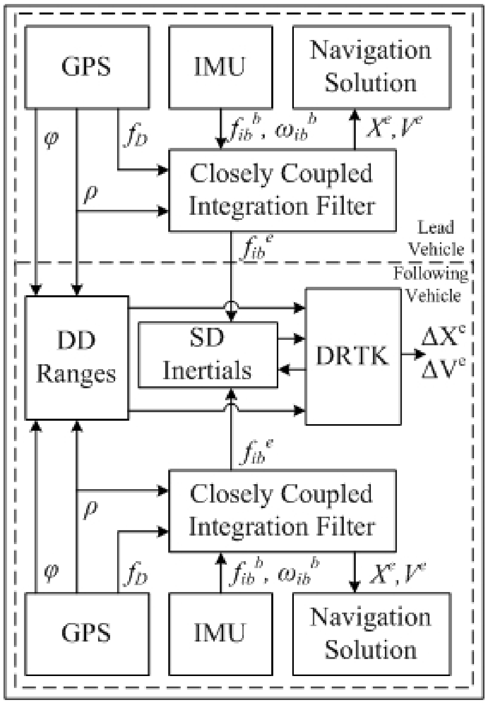

Fig. 4 Closely coupled

taining the relative specific force as an input is expressed as follows:

$$\begin{aligned}\vec{r}_{AB_k} &= \vec{r}_{AB_{k-1}} + \dot{\vec{r}}_{AB_{k-1}}\Delta t \\ &+ \left(\Delta f^e_{AB_k} - b_{\Delta f_k}\right)\frac{\Delta t^2}{2}\end{aligned} \tag{36}$$

The estimated state vector contains the RPV and relative velocity between the vehicles, the bias terms, and the double differenced phase ambiguities.

$$X = \begin{bmatrix}\vec{r}_{AB} & \dot{\vec{r}}_{AB} & b_{\Delta f} & \nabla\Delta N\end{bmatrix}^T \tag{37}$$

The estimates and error covariance are propagated forward in time with

$$X_k = \Phi_k X_{k-1} + \Gamma \Delta f^e_k \tag{38}$$

$$P^-_k = \Phi_k P^+_{k-1}\Phi^T_k + Q \tag{39}$$

where the state transition matrix is

$$\Phi = \begin{bmatrix} I_3 & \Delta t I_3 & -\frac{\Delta t^2}{2} I_3 & 0 \\ 0 & I_3 & -\Delta t I_3 & 0 \\ 0 & 0 & I_3 & 0 \\ 0 & 0 & 0 & I_m \end{bmatrix} \tag{40}$$

input gain matrix is

$$\Gamma = \begin{bmatrix}\frac{\Delta t^2}{2} I_3 & \Delta t I_3 & 0 & 0\end{bmatrix}^T \tag{41}$$

The process covariance was approximated by neglecting off diagonal terms as follows:

$$Q = diag\left(\begin{bmatrix}\sigma^2_{\Delta f^e}\Delta t & \sigma^2_{\Delta f^e} & \sigma^2_{b_{\Delta f^e}} & 0\end{bmatrix}\right) \tag{42}$$

The measurement vector was formed using Equations 13 and 14 with L1 and L2 data.

$$z = \begin{bmatrix}\nabla\Delta\rho_{L1} & \nabla\Delta\rho_{L2} & \nabla\Delta\phi_{L1} & \nabla\Delta\phi_{L2}\end{bmatrix}^T \tag{43}$$

The measurement matrix contained single differenced unit vectors; the base unit vector was removed from all other unit vectors from one receiver.

$$H = \begin{bmatrix} \Delta e^s_A & 0 & 0 & 0 \\ \Delta e^s_A & 0 & 0 & 0 \\ \Delta e^s_A & 0 & \lambda_{L1} I_m & 0 \\ \Delta e^s_A & 0 & 0 & \lambda_{L2} I_m \end{bmatrix} \tag{44}$$

The measurement covariance accounted for the correlation injected by the double difference operation. No correlation was include between L1 and L2 data, or between range and phase data. The algorithm proceeds with a measurement update when time synchronized data is available from two receivers.

$$K = P^-_k H^T \left(H P^-_k H^T + R\right)^{-1} \tag{45}$$

$$X^+_k = X^-_k + K\left(z - H X^-_k\right) \tag{46}$$

$$P^+_k = (I_{17} - KH) P^-_k \tag{47}$$

The estimated ambiguities are fixed to integer values at this point in the algorithm. However, the focus of this work remains on the improvements to the floating solution. Future work will assess the effects on ambiguity fixing.

RESULTS

Two NovAtel PropakV-3's and Crossbow IMU440's were mounted separately in two vehicles. A Septentrio PolaRx2e dual frequency receiver and radio modem installed at the base station provided corrections to the NovAtel receivers. The range and inertial data was recorded for post processing, and the RTK position of each vehicle was logged at 1 Hz to serve as a truth measurement. The vehicles were driven in a convoy formation around Auburn University's 1.7 mile test track. Speeds started at 20mph and increased in 10mph increments to 50mph after the completion of each lap around the course. Figure 5 is a plot of the test path. The data was processed in the DRTK/INS algorithm to produce a 50 Hz RPV. The baseline between the vehicles is shown in Figure 6. The RTK positions of the vehicles were differenced to determine a "true" RPV between the vehicles.

Figure 7 displays the estimated and measured RPV between the vehicles as they traveled around the track. The ECEF frame served as the navigation frame; blue is the relative distance in X, red is the relative distance in Y, and green is the relative distance in Z.

Detailed versions of Figures 6 and 7 are given in Figures 8 and 9. It can be seen that the RPV estimate using the

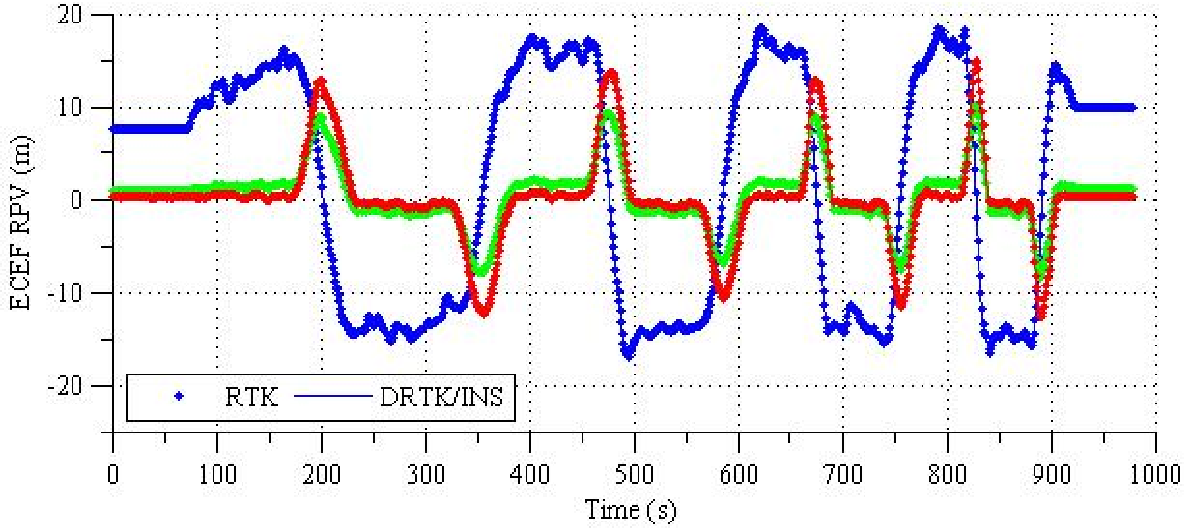

Fig. 7 The estimated and measured relative position vector is shown. Blue is ECEF X, red is ECEF Y, and green is ECEF Z.

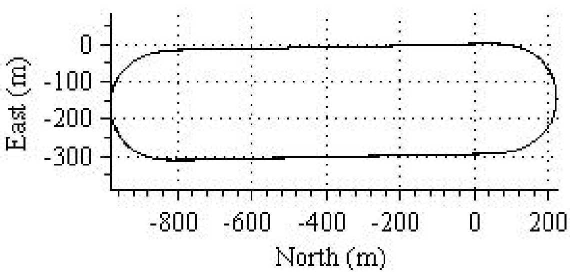

Fig. 5 Auburn University's 1.7 mile oval test track was used as a test course.

floating point ambiguities tracks the relative motion of the vehicles, indicated by the differenced RTK positions.

Full GPS outages lasting ten seconds were simulated at seven arbitrarily chosen times during separate trials using the same data as the above plots. The time where each solution drifted beyond 10cm from truth was recorded. The drift time was inconsistent between outages, which was to be expected due to the nonlinearities Equations 15 through 22. The shortest time recorded was 1.16 seconds, and the longest time was still within 10 cm after the outage ended. The mean outage time 3.97 seconds, which given the fact the Crossbow IMU440 is an automotive grade IMU, and measurements from two IMUs were combined, this is in line with the results presented in [9]. Table 3 contains the recorded times the solution took to drift over 10 cm.

CONCLUSIONS

This paper has described the reasoning behind and methodology of a closely coupled relative GPS/INS system used to accurately estimate the relative position between two dynamic receivers. The pseudo-range and pseudo-range rate were used to calibrate and rotate an IMU's measurements into the ECEF frame. Two aligned IMUs were combined with relative pseudo-range and carrier phase measurements to estimate a relative position, velocity, and phase ambiguities at a high rate.

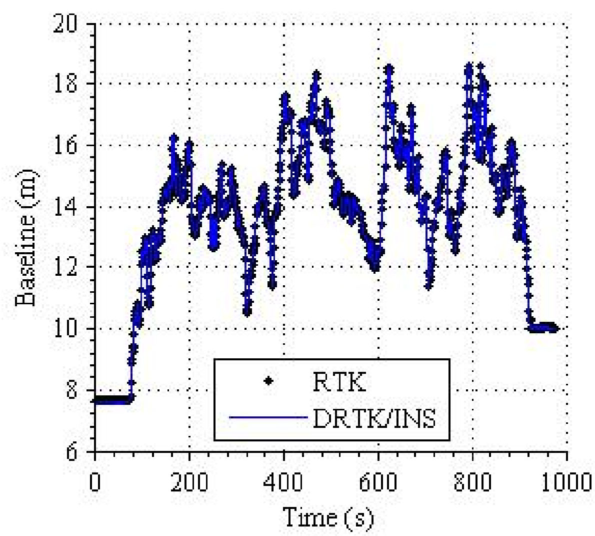

Fig. 6 The magnitude of the separation distance between the vehicles as they traveled around the track at 10, 20, 30, 40, and 50 mph is shown.

Preliminary analysis of the algorithm showed an increase in robustness to common sources of error experienced on ground vehicles. A high rate RPV was generated that was capable of bridging short GPS outages. The mean time to drift 10 cm from the true baseline was determined to be 3.97 seconds using seven simulated outages.

Future work will focus on assessing the improvement, if

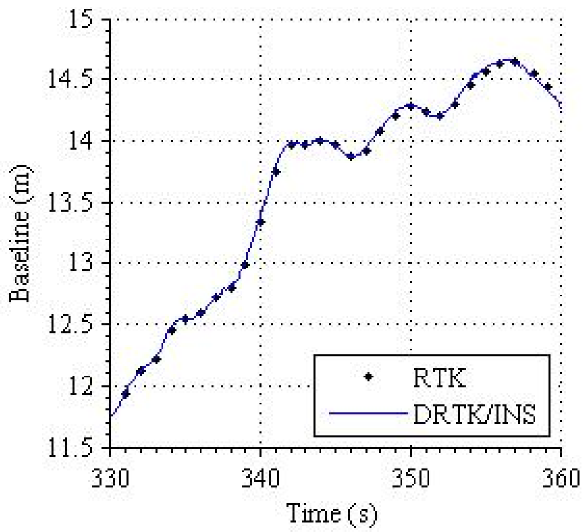

Fig. 8 A closeup of Figure 6 is displayed, which shows the baseline between the two moving vehicles.

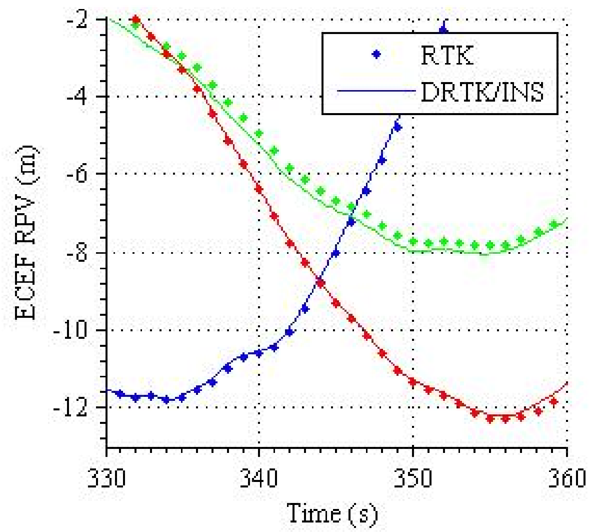

Fig. 9 A close up of the RPV measurement and estimate is shown. Blue is ECEF X, red is ECEF Y, and green is ECEF Z.

Table 3 Time to 10cm Error

Start Time (s)	End Time (s)	Duration (s)
188.64	192.52	3.88
268.62	278.62	10+
318.62	326.00	7.38
433.64	435.20	1.56
478.66	481.44	2.78
603.40	606.04	2.64
813.64	814.80	1.16
948.74	951.08	2.34

any, to ambiguity resolution. Several more integration routines will be considered, and then compared to determine the most feasible system for a series of ground vehicles.

ACKNOWLEDGMENTS

The authors would like to thank TARDEC for their support of this work and Buzz Powell at the National Center for Asphalt Technology (NCAT) for use of the test track.

REFERENCES

[1] W. Travis and D. M. Bevly, "Trajectory duplication using relative position information for automated ground vehicle convoys," in *Proceedings of IEEE/ION Postion, Location, and Navigation Symposium*, May 2008, pp. 1022 – 1032.

[2] S. J. Comstock, "Development of a low-latency, high data rate, differential gps relative positioning system for uav formation flight control," Ph.D. dissertation, Air Force Institute of Technology, 2006.

[3] S. Felter and N. Wu, "A relative navigation system for formation flight," *IEEE Transactions on Aerospace and Electronic Systems*, vol. 33, pp. 958–967, 1997.

[4] S. Khanafseh, B. Kempny, and B. Pervan, "New applications of measurement redundancy in high performance relative navigation systems for aviation," *Proceedings of the 19th International Technical Meeting of the Satellite Division of the Institute of Navigation ION GNSS 2006*, pp. 3024–3034, 2006.

[5] S. Khanafseh, "Gps navigtional algorithms for autonomous airborne refuling of unmanned air vehicles," Ph.D. dissertation, Illinois Institute of Technology, May 2008.

[6] S. Dogra, J. Wright, and J. Hansen, "Sea-based jpals relative navigation algorithm development," *Proceedings of the 18th International Technical Meeting of the Satellite Division of the Institute of Navigation ION GNSS 2005*, pp. 2871–2881, 2005.

[7] T. Ford, M. Hardesty, and M. Bobye, "Helicopter ship board landing system," in *ION GNSS 18th International Technical Meeting of the Satellite Division*, 2005.

[8] M. Petovello, G. Lachapelle, and M. Cannon, "Using gps and gps/ins systems to assess relative antenna motion onboard an aircraft carrier for shipboard relative gps," *Proceedings of the 2005 National Technical Meeting of the Institute of Navigation*, pp. 219–229, 2005.

[9] H. Zhang, M. Petovello, and M. Cannon, "Performance comparison of kinematic gps integrated with different tactical level imus," in *Proceedings of the*

2005 National Technical Meeting of the Institute of Navigation, January 2005.

[10] P. Misra and P. Enge, *Global Positioning System: Signals, Measurements, and Performance*. Ganga-Jamuna Press, 2006.

[11] B. Hofmann-Wellenhof, H. Lichtetnegger, and J. Collins, *GPS: Theory and Practice*. Springer-Verlag, 2001.

[12] E. D. Kaplan and C. J. Hegarty, *Understanding GPS: Principles and Applications*, E. D. Kaplan and C. J. Hegarty, Eds. Artech House, Inc., 2006.

[13] B. W. Parkinson, Ed., *Global Positioning System: Theory and Applications Volume II*. American Institute of Aeronautics and Astronautics, 1996.

[14] R. Kroes, "Precise relative positioning formation flying spacecraft using gps," Ph.D. dissertation, Delft University of Technology, 2006.

[15] P. de Jonge and C. Tiberius, "The lambda method for integer ambiguity estimation: Implementation aspects," Delft Geodetic Computing Centre, Tech. Rep., August 1996.

[16] B. W. Parkinson, Ed., *Global Positioning System: Theory and Applications Volume I*. American Institute of Aeronautics and Astronautics, 1996.